
DTU-Net: Learning Topological Similarity for Curvilinear Structure Segmentation

Manxi Lin

Technical University of Denmark
manli@dtu.dk

Zahra Basir

CAMES, Rigshospitalet
zab@regionsjaelland.dk

Martin Grønnebak Tolsgaard

CAMES, Rigshospitalet
martintosgaard@gmail.com

Anders Nymark Christensen

Technical University of Denmark
anym@dtu.dk

Aasa Feragen

Technical University of Denmark
afhar@dtu.dk

Abstract

Curvilinear structure segmentation plays an important role in many applications. The standard formulation of segmentation as pixel-wise classification often fails to capture these structures due to the small size and low contrast. Some works introduce prior topological information to address this problem with the cost of expensive computations and the need for extra labels. Moreover, prior work primarily focuses on avoiding false splits by encouraging the connection of small gaps. Less attention has been given to avoiding missed splits, namely the incorrect inference of structures that are not visible in the image.

In this paper, we present DTU-Net, a dual-decoder and topology-aware deep neural network consisting of two sequential light-weight U-Nets, namely a texture net, and a topology net. The texture net makes a coarse prediction using image texture information. The topology net learns topological information from the coarse prediction by employing a triplet loss trained to recognize false and missed splits, and provides a topology-aware separation of the foreground and background. The separation is further utilized to correct the coarse prediction. We conducted experiments on a challenging multi-class ultrasound scan segmentation dataset and an open dataset for road extraction. Results show that our model achieves state-of-the-art results in both segmentation accuracy and continuity. Compared to existing methods, our model corrects both false positive and false negative examples more effectively with no need for prior knowledge.

1 Introduction

Curvilinear structures represent thin and long objects in images Bibiloni et al. (2016), and their segmentation has extensive application in computer vision and medical imaging, e.g., road extraction for route planning Wang et al. (2022); Xu et al. (2021); Zhang et al. (2018), segmentation of anatomical networks L Srinidhi et al. (2017); Li et al. (2020); Mou et al. (2021), and pavement crack detection Cubero-Fernandez et al. (2017); Safaei et al. (2022); Yusof et al. (2018).

Segmentation of curvilinear structures is inherently challenging due to their thin and long shapes: Their connectivity can be significantly altered even just by a small number of incorrectly classified

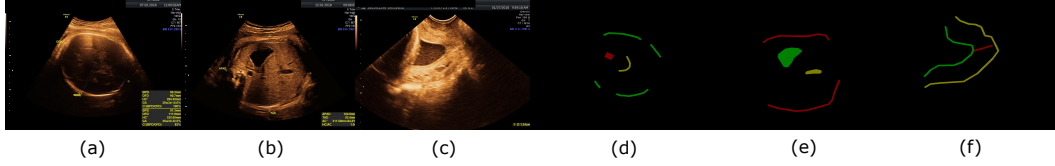


Figure 1: Examples of volumetric and curvilinear structures in ultrasound images of fetal head and abdomen, as well as cervix, shown in (a), (b) and (c) respectively. The corresponding manual segmentations are shown in (d), (e), and (f). Note how the images contain both curvilinear and volumetric structures. Please zoom in for details.

pixels. The segmentation problem becomes even more challenging in images with low contrast or low resolution, where the curvilinear structure is less distinguishable from the background. As a result, connectivity errors due to incorrectly splitting curves (we term these "**false splits**") and incorrectly connecting them ("**missed splits**"), are very common.

In this paper, we consider curvilinear segmentation problems where missed splits are just as harmful as false splits. This is in contrast with existing literature Clough et al. (2019); Shit et al. (2021); Xu et al. (2021), which most often focuses on avoiding false splits, leading to a bias towards overly connected structures. Our focus on missed splits is in part motivated by image quality assessment in fetal ultrasound Wu et al. (2017), where a requirement for sufficient image quality is for particular organs to be completely visible in the image. In this application, a bias towards oversegmentation is directly harmful. Additionally, we draw motivation from road network segmentation, where downstream applications such as route planning would similarly suffer from missed splits. Figure 1 illustrates some examples of curvilinear objects in ultrasound, as well as their annotations for segmentation tasks.

To address the above mentioned challenges, we make the following contributions:

1. We propose a dual-decoder neural network for curvilinear structure segmentation, with a two-stage prediction based on image texture and topology, respectively. The refined prediction is generated by fusing the two predictions softly.
2. Utilizing deep contrastive learning, we leverage the latent embedding similarity to learn topological information of the images in an end-to-end scheme, which does not rely on any prior information and produces self-supervised embeddings that respect the curvilinear structure topology.
3. We demonstrate the effectiveness of our model on a challenging multi-class ultrasound scan segmentation task and the open Massachusetts Road Extraction dataset.

2 Related Work

Curvilinear structure segmentation. Early geometric methods detected curvilinear structures by modeling their geometrical properties, which have poor performance under low contrast Frangi et al. (1998); Sato et al. (1998). With the rise of deep learning, convolutional neural networks (CNNs) have shown impressive performance in curvilinear structure segmentation Li et al. (2020); Mou et al. (2021). Besides the common network architectures adopted in general segmentation tasks Ronneberger et al. (2015); Chen et al. (2017); Long et al. (2015), e.g., U-Net, some works Jha et al. (2020); Wang et al. (2022); Mou et al. (2021); Li et al. (2020) design delicate backbones and schemes designed to capture the details of curvilinear features. CS-Net Mou et al. (2021) introduces the self-attention mechanism and deals with multiple curvilinear types in a unified manner. IterNet Li et al. (2020) concatenates multiple U-Nets to incorporate the structural redundancy. Nevertheless, these methods, which simply learn semantic labels per pixel, often fail to preserve the connectivity of objects.

An alternative is given by post hoc approaches Sasaki et al. (2017); Wang and Jiang (2018); Vega et al. (2015) which correct the broken predictions from an independent segmentation model. Sasaki et al. Sasaki et al. (2017) proposed an auto-encoder that detects and paints the gaps in images automatically. Wang et al. Wang and Jiang (2018) extracted the skeleton of the segmented images

and remove spurious vessels by morphological erosion. These post hoc methods have in common that they only refine the coarse predictions obtained from other models, usually by looking only at the coarse prediction, not the image. Thus, such models are impotent when the coarse predictions are of low accuracy, and they come with a risk of inpainting structures which are not actually visible in the image. Moreover, the post processing adds an extra layer of computations.

Another branch of research aims to Clough et al. (2019); Zhang and Lui (2022); Hu et al. (2019) correct the image topological information by enforcing a ground truth, or prior, topology. Clough et al. (2019) used persistent homology as the measure of prediction topology, which requires expensive topological computation and only considers simple topological structures. TPSN Zhang and Lui (2022) deforms a binary mask describing the topology priors for making topology-preserving segmentation. These methods become challenging and expensive to use when the curvilinear structure has a complicated topology. They also do not apply in situations where the topology is not known beforehand. In particular, they do not apply to tasks where the goal of segmentation is, indeed, to discover the topology of the structure at hand.

Recent works Shit et al. (2021); Xu et al. (2021); Chen et al. (2020); Mosinska et al. (2018) investigate the prior-free preservation of topology in curvilinear segmentation. TR-GAN Chen et al. (2020) is a generative adversarial network that improves artery/vein classification of vessels by improving the segmented vessel connectivity. This is done using a topology ranking discriminator together with a contrastive loss encouraging the network to avoid missed splits. The topological features learned by a pre-trained network are only involved in the computation of cost functions to preserve the image topology. Shit et al. (2021) segment curvilinear structures which are obtained as skeletons from thin volumetric annotations. Based on the skeletons, the cIDice loss function is designed to encourage the segmentations to maintain correct topology. These methods are the closest to our proposed method, in the sense that they also address, at least implicitly, both false splits and missed splits. Our experiments include an extensive comparison with cIDice, which is shown to struggle, in particular, on the low image quality ultrasound images.

Deep contrastive learning. Contrastive learning is typically used to extract effective instance features for downstream tasks. Deep contrastive learning teaches CNNs to produce embeddings that keep similar objects close, and push dissimilar objects apart, for instance by pulling together instances with the same label and pushing away the instances of different labels. FaceNet Schroff et al. (2015) proposes a triplet loss for human face recognition. The triplet loss considers the face similarity with positive and negative examples, and maximizes the similarity difference. Following works Hermans et al. (2017); Dong and Shen (2018) incorporate the triplet loss into object detection and person re-identification tasks, and achieve impressive performance. These works, however, usually require annotations indicating positive and negative examples. In this paper, we adopt the triplet loss for self-supervised learning of image topology features. Our method generates positive and negative examples from segmentation ground truth online during training, and does not need additional annotations.

3 Method

In section 3.1, we first briefly revisit topology preservation in curvilinear segmentation, which motivates our topology-aware network, DTU-Net. Then we present the architecture and workflow of DTU-Net. Section 3.2 describes the details of the topology net, the most important component in our DTU-Net that learns object topology. Last, we introduce our prediction refinement strategy in section 3.3.

3.1 Decoupling Topology-preserving Curvilinear Segmentation

Image segmentation is most often formulated as a pixel-wise classification task based on image texture. However, this is not enough to capture complete curvilinear structures in the image, as small pixel-wise errors can lead to incorrect connectivity. We endorse the use of topological information in segmentation that helps model the object connectivity. Topological loss functions such as cIDice Shit et al. (2021) or topoloss Clough et al. (2019) seek to train networks to explicitly avoid breaking topological structure.

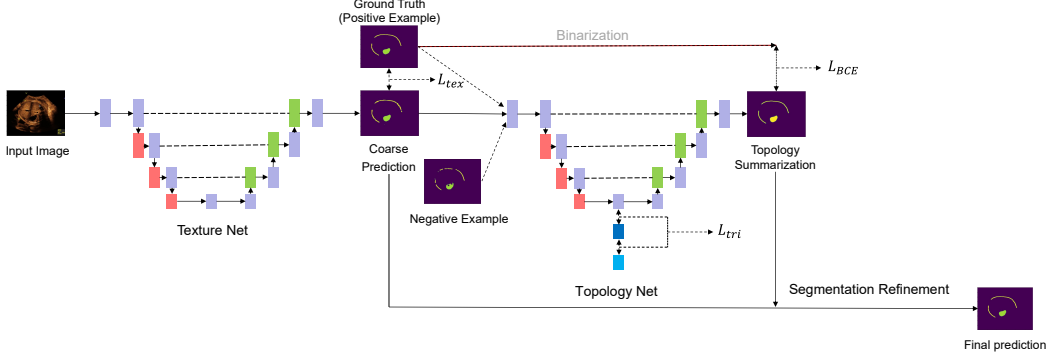


Figure 2: Network architecture of DTU-Net. The dotted arrows refer to operations that only performed at training stage. Please zoom in for details.

However, we argue that this ambitious goal, i.e., preserving topology and encoding image textures at the same stage, can make the model hard to tune, especially on images with low contrast or resolution. Thus, in this paper, we address curvilinear in a two-stage manner, splitting the topology-preserving curvilinear segmentation into two simpler sub-tasks: learning texture information, and learning topological information from the texture-based coarse segmentation.

Figure 2 presents the **Dual-decoder and Topology-aware U-Net (DTU-Net)** architecture. Our DTU-Net includes two lightweight mini U-Nets, which we refer to as the texture net and the topology net. The texture net is a mini U-Net with a smaller number of layers than the original U-Net. It follows the learning scheme of most general segmentation tasks - encoding image texture information and giving pixel-wise predictions. The coarse prediction from the texture net is further fed to the topology net for topology preservation. The topology net is another mini U-Net, where the encoder learns topological features using a self-supervised triplet loss, and the decoder summarizes the topology in a binary segmentation map indicating image foreground and -background. The texture-based and topology-based predictions are further softly fused to obtain the final segmentation.

Note that in practice, the texture net can be replaced with any pre-trained or randomly-initialized segmentation network. This means that our model can be also employed as an easy-to-use plugin to extend to powerful general segmentation models. Our use of light-weight mini-U-nets is motivated by the ultrasound image quality assessment task, where we aim to use segmentation to provide real-time feedback on image quality with limited computational resources.

3.2 Topology Net

Learning topological embedding with triplet Loss Recent works Chen et al. (2020); Mosinska et al. (2018) adopt a pre-trained VGG19 network Simonyan and Zisserman (2014) to extract high-level image topological features and constrain the segmentation by contrastive losses, which penalize predictions with different topological features from the ground truth. In these methods, topological information is extracted by models pre-trained on natural images Deng et al. (2009), which is agnostic to the task. In addition, during training, only the feature differences are considered instead of the features themselves.

We leverage the encoder of a mini U-Net $\Psi(\cdot)$ to extract image topological features. $\Psi(\cdot)$ is trained with the triplet loss, which takes an anchor, a positive and a negative example as input, and penalizes the difference of anchor distance to the positive example that from the same category, with the anchor distance to the negative example that from the same category. We consider the category to be object topology here. Our $\Psi(\cdot)$ is trained in a self-supervised manner by forwarding three inputs with shared parameters: the coarse prediction $\Theta(I)$ (the pixel-wise probability given by the texture net $\Theta(\cdot)$), the segmentation ground truth mask G which has naturally the correct topology, and a corrupted mask \hat{G} where the connectivity is deliberately broken by us. As the coarse prediction has values from 0 to 1, both the ground truth mask and the corrupted mask are converted to one-hot embedding. Sequentially, the triplet loss is defined as:

$$L_{tri}(\Psi(\Theta(I)), \Psi(G), \Psi(\hat{G})) = \max(d^+ - d^- + 0.1, 0) \quad (1)$$

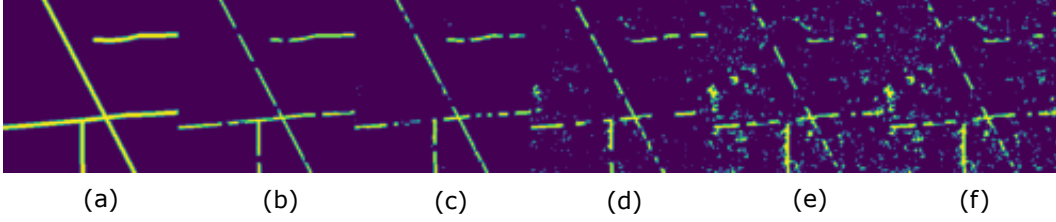


Figure 3: An example of generated masks under different λ values. (a) is a road network mask randomly cropped from Mnih (2013). (b) to (f) refers to the generated mask when $\lambda = 0.1, 0.2, 0.3, 0.4$, and 0.5 .

where d^+ is the averaged second-order pixel-wise feature difference of $\Psi(\Theta(I))$ and $\Psi(G)$, d^- is the difference of $\Psi(\Theta(I))$ and $\Psi(\hat{G})$ and 0.1 is an empirically-set margin. By minimizing the triplet loss during training, the network forces the image features closer to the features of the ground truth segmentation mask whose topology is correct, while simultaneously pushing it further away from the embedding of the corrupted segmentation masks.

Self-supervised training of the triplet loss We generate the corrupted masks from the ground truth mask by randomly breaking the image topology. The false splits and missed splits are considered separately. On the one hand, as the curvilinear structures are challenging to capture, the false splits can happen anywhere on the curves when the CNNs fail to recognize the objects. Therefore, we split the segmentation labels into small patches, and randomly remove λ of the patches containing foreground information, where $\lambda \in [0, 1]$ is a hyper parameter controlling the corruption degree. On the other hand, we deem the missed splits tend to appear in regions with similar texture features, put simply in raw images, the pixel values. We compute the average m and standard deviation d of the foreground pixel values in the image (foreground pixels are given in the ground truth). λ of the pixels with value within $[m - d, m + d]$ are picked randomly and assigned with the label of the most similar foreground pixel. In practice, adding missed splits and false splits is done sequentially. Figure 3 shows a ground truth mask and the corrupted examples with different severity. According to the figure, the curves are more naturally broken as the false splits are added by patches instead of simply dropping out pixels. The introduction of missed splits brings not only the incorrect connection between curves but also the noises, which harms the topology as well.

During inference, the encoder only forwards $\Psi(\Theta(I))$. The triplet loss in Eq. 1 quantifies the pixel-wise feature difference. We also merge the global topological feature into the embedding by a SENet Hu et al. (2018), which takes the average of the learned feature map and encodes them into attentive scores via a multi-layer perceptron. The scores are then multiplied with the original feature map.

Fine-to-coarse topology summarizing. Compared to the existing methods adopting pre-trained models, our topology encoder is trainable and the learned topological features are further used in the decoder of the topology net. Specifically, the decoder aims at converting the topology knowledge into a form that is useful for the curvilinear segmentation task.

In our DTU-Net, the texture net learns low-level information directly from raw images, which is effective in semantic segmentation tasks. Our topology net, however, abstracts the information into high-level topological features, which is hardly applicable for the texture recognition tasks due to the loss of texture details. We expect the topology net to summarize the information from object connectivity, and contributes to the final segmentation. Consequently, we ask the topology net yet a simple question - based on the learned topology, whether the pixel should be connected or not? In other words, our topology network is addressing a binary segmentation task splitting the foreground and background pixels. The binary predictions are sequentially employed to refine the semantic segmentation from the texture net.

3.3 Segmentation Refinement and Joint Feature Learning

Our DTU-Net consists of a texture network and a topology network. We denote the texture network, the encoder and the decoder of the topology network as $\Theta(\cdot)$, $\Omega(\cdot)$ and $\Psi(\cdot)$ respectively. Each part

Table 1: Results on the ULTRASOUND dataset. Here, we compare the performance of our method to the baselines on a range of metrics.

Settings		Geometric	Topological				Pixel-wise	
Model	Loss	Frechet	TopErr	#Images TopErr	#Images MS	#Images FS	Acc	mAcc
mini U-Net	clDice	0.7801	0.2635	146	88	144	79.45	76.09
IterNet	focal	0.4329	1.0963	207	137	144	7.16	4.59
inpainting	MSE	0.8189	1.1179	201	87	201	80.49	72.10
DTU-Net	Eq. 2	0.5818	0.0974	98	70	77	86.39	82.23

Table 2: Results on the ROAD dataset, comparing the same baselines as above.

Settings		Geometric	Topological				Pixel-wise		
Model	Loss	Frechet	TopErr	#Images TopErr	#Images MS	#Images FS	Acc	Recall	Precision
mini U-Net	clDice	785.1	0.3965	49	49	49	96.55	95.5	97.23
IterNet	focal	783.4	0.253	49	49	49	95.75	97.98	93.44
inpainting	MSE	783.4	0.4232	49	49	49	95.5	97.71	93.19
DTU-Net	Eq. 2	786.7	0.3969	49	49	49	96.76	96.29	96.9

of the network can be trained separately, which is similar to the post hoc methods. We train the network in a joint way, where the gradient back propagation from the topology net can also update the parameters in the texture net. Given the input image as I and the segmentation ground truth mask G , DTU-Net is trained by a unified loss

$$L_{DTU}(I, G) = L_{tex}(\Theta(I), G) + L_{BCE}(\Omega(\Psi(\Theta(I))), \bar{G}) + L_{tri}(\Psi(\Theta(I)), \Psi(G), \Psi(\hat{G})) \quad (2)$$

where L_{tex} is the pixel-wise segmentation loss for the texture net, L_{BCE} is the binary cross entropy loss tuning the prediction from the topology net, L_{tri} is the triplet loss, \bar{G} and \hat{G} refers to the ground truth binarized and corrupted by us. The loss function also indicates that our DTU-Net does not need additional annotations and learns image topology in a self-supervised way.

As the topology net and the texture net views the segmentation problem in different angles, we fuse their predictions to get a complete view of the segmentation task. The last stage of our DTU-Net is to refine the coarse semantic prediction with the topology-aware binary prediction. Innovated by ensemble learning Schapire (1999); Li et al. (2008), we fuse the two predictions by weighted summation. We weight the predictions by a hyper parameter ω , which indicates our confidence on the texture-based prediction. For each pixel, given $p_{top}^{(i)}$ the pixel-wise probability of the i -th category from the topological prediction, and $p_{tex}^{(i)}$ the pixel-wise probability of the i -th category from the textural prediction, the two predictions are simply fused by:

$$p_{final}^{(i)} = \begin{cases} (1 - \omega)(1 - p_{top}^{(0)}) + \omega p_{tex}^{(0)}, & i = 0; \\ \frac{(1 - \omega)p_{top}^{(0)} + \omega \sum_{i=1}^c p_{tex}^{(i)}}{\sum_{i=1}^c p_{tex}^{(i)}} p_{tex}^{(i)}, & i = 1, 2, \dots, c \end{cases} \quad (3)$$

where c is the total number of categories in the semantic segmentation task, $p_{final}^{(i)}$ is the pixel-wise final prediction, the 0-th category means the background.

4 Experiments

We perform experiments on two different datasets, comparing the performance of our model to a range of different baselines.

Baseline models. We compare the performance of our model against a mini U-net trained with the clDice loss function, as well as with IterNet Li et al. (2020) and the inpainting network of Sasaki

Table 3: cIDice model selection on the ROAD dataset.

Settings	Geometric	Topological				Pixel-wise		
α	Frechet	TopErr	#Images TopErr	#Images MS	#Images FS	Acc	Recall	Precision
0	757.9	0.3613	49	8	49	96.28	96.43	95.8
0.2	785.1	0.3965	49	49	49	96.55	95.5	97.23
0.4	785.1	0.3987	49	8	49	96.53	95.41	97.26
0.6	759.5	0.4006	49	32	49	96.21	95.44	96.58
0.8	786.7	0.4434	49	15	49	95.5	95.71	94.91
1	783.4	1.18	49	49	49	17.35	3.18	4.09

Table 4: cIDice model selection on the ULTRASOUND dataset. In the first two rows, we find the suggested models used in the original paper Shit et al. (2021); these did not converge. In the following rows, we find results for various parameters using the focal loss in place of the softdice.

Settings		Geometric	Topological				Pixel-wise	
α	β	Frechet	TopErr	#Images TopErr	#Images MS	#Images FS	Acc	mAcc
0	0.5	-	9.8019	210	32	210	0.84	7.4
0	1	-	13.93	210	9	210	6.55	7.7
0	0	0.8418	0.4572	161	117	161	98.8	74.14
0.2	0	0.7801	0.2635	146	88	144	99.09	84.37
0.4	0	1.0727	0.3873	158	106	158	98.9	79.09
0.6	0	0.8959	0.3099	152	98	151	99	82.85
0.8	0	1.1894	0.6699	170	123	169	98.61	61.49
1	0	-	15.4591	210	8	210	6.18	7.68

et al. (2017). The input of the inpainting network is the prediction from a mini U-Net trained by a focal loss.

The cIDice loss function preserves topological information by learning object skeletons, which, however does not guarantee accurate segmentation. In the original paper Shit et al. (2021), this is handled by mixing the cIDice metric with another pixel-wise classification loss, more precisely the soft dice loss:

$$L_{clDice} = \beta(1 - clDice) + (1 - \beta)(1 - softDice) \quad (4)$$

where β is a hyper parameter.

In our experiments – in particular on the more challenging ultrasound dataset – we found the cIDice loss function challenging to tune. For us, the experimental setup from Shit et al. (2021) did not converge with either of the suggested values of $\beta = 0$ or 0.5 (see Table4). To improve convergence, we replaced softDice with focal loss Lin et al. (2017):

$$L_{clDice} = \alpha(1 - clDice) + (1 - \alpha)L_{focal}. \quad (5)$$

Even here, however, the performance was unstable with the choice of α , as can be seen from Table 4, and we choose to compare to the optimal observed $\alpha = 0.2$ in Table 1. For the road extraction task, we did the similar selection (see Table 3) and also choose $\alpha = 0.2$ in Table 2.

Dataset We validate our results on two datasets. On the ULTRASOUND dataset we consider a challenging ultrasound segmentation task aiming to delineate both volumetric and curvilinear structures. The dataset consists of images obtained for a typical growth scan from the 3rd trimester of a pregnancy, where four standardized ultrasound images are acquired in order to predict the size of the fetus. These images are standardized via the visibility of a fixed set of anatomical organs, several of which appear as curvilinear structures in the image. Here, it is important for the segmentation algorithm to accurately detect whether the entire structure is actually present, as well as to measure their dimensions. There are 2088 images in the dataset, accrossing 6 curvilinear structures and 7

blob-shaped categories. Each image has a resolution of 960×720 . The images were divided into 80% for training, 10% for validation and 10% for testing.

As a typical prediction task would be to segment multiple different organs realtime while scanning, we have trained our models to segment both the volumetric and curvilinear structures in all four standardized images usually acquired (head, abdomen, femur, cervix). In Table 1 we only report accuracy on the curvilinear objects.

We conducted the road extraction experiments on the ROAD dataset Mnih (2013), which includes 1108 images for training, 14 images for validation and 49 images for testing. The road extraction task only needs to separate foreground from the background, yet the road networks usually have very complicated topology. In the road extraction problem, the missed splits are also as harmful as false splits, as it affects the downstream tasks such as route planning significantly.

Hyper parameter and experimental settings. To train the texture net, we adopt a combination of dice loss and focal loss as L_{tex} in Eq. 2. On both two datasets, we generate the examples for the triplet loss incrementally. At the first 20 epochs, the hyper parameter λ is set 0.5, which means 50% foreground pixels are randomly removed and 50% texture-similar noises are added into the mask. We increase the difficulty of discriminating positive and negative examples during the training to force the topology encoder learning effective features gradually. Specifically, we decrease λ by 10% every 20 epochs to generate the negative examples more and more indiscriminate to the ground truth mask. ω in Eq. 3 is set 0.5 and 0.3 for the ULTRASOUND and ROAD dataset respectively. We describe detailed experimental settings in the supplements.

Evaluation metrics. In this paper, our primary interest is to create connected curvilinear structures when this is supported by the images – and to avoid it when it is not. To this end, we seek to quantify both the topological correctness of the segmented structures, as well as the geometric affinity between the predicted and annotated curves.

To measure geometric affinity between curves, we employ the Frechet distance Alt and Godau (1995), which measures the extent to which the two curves remain close to each other throughout their course. This is a far more suitable metric than e.g. accuracy, which is very sensitive to small shifts or differences in curve thickness.

To measure topological correctness of the segmented structures, we apply a sliding window to measure local topological correctness within image patches. Within the sliding window, we count the difference between number of components in the prediction and the ground truth annotation, respectively. This corresponds to a local Betti number computation. For each image, we compute a topological error (TopErr) which is just the average difference over all patches seen. To further assess how frequently topological errors occur, we also report the number of images with topological error. Finally, to assess whether the topological errors consist of incorrectly splitting curves (false split), or incorrectly joining a curve that should be split (missed split), we count how many images have at least one patch-wise false split, or missed split, respectively.

For completeness, we also include some of the standard voxel-wise metrics, more precisely accuracy and mean class accuracy, both overall and restricted to the curvilinear structure classes in the multi-class segmentation problem. For the binary segmentation task, we leverage the recall and precision to replace the class-average accuracy.

Ablation Study We conducted an ablation study over different components of the proposed DTU-Net on the ULTRASOUND dataset. Table 5 records the result. We remove the triplet loss from Eq 2 to verify the topology encoding. We also evaluate the effectiveness of feature fusion. Specifically, ω in Eq 3 is set to be 0 and 1 respectively, meaning that the prediction of foreground and background is dominated by the topology net or the texture net. In addition, we revise the output channel number of topology net to produce multi-class predictions directly. To prove that our model performance is not merely due to the increase of learnable parameters, we also include a comparison with a larger U-Net trained with the cIDice loss ($\alpha = 0.2$), which has roughly two times the model size of ours (Table 6).

Results For the ULTRASOUND dataset, results are found in Table 1. For the ROAD dataset, results are presented in Table 2. Figure 4 illustrates an example of the segmentation results. We include more visualizations on both ULTRASOUND and ROAD dataset in supplements.

Table 5: Ablation study on different components of DTU-Net

Settings	Geometric	Topological				Pixel-wise	
Model	Frechet	TopErr	#Images	#Images	#Images	Acc	mAcc
w/o triplet loss	0.6605	0.1056	99	69	68	86.36	81.53
$\omega = 0$	0.5863	0.1023	101	84	57	82.40	78.40
$\omega = 1$	0.8601	0.1683	131	89	123	83.40	80.08
pure topology decoder	1.1016	0.5730	168	119	167	67.06	53.71
DTU-Net	0.5818	0.0974	98	70	77	86.39	82.23

Table 6: Ablation on Model size

Settings		Geometric	Topological				Pixel-wise	
Model	Size	Frechet	TopErr	#Images TopErr	#Images MS	#Images FS	Acc	mAcc
full U-Net	131.8M	0.5849	0.1383	126	75	113	83.68	78.9
DTU-Net	65.5M	0.5818	0.0974	98	70	77	86.39	82.23

5 Discussion and Conclusion

We have designed a framework for curvilinear structure segmentation which prioritizes not only to avoid false splits, but also to avoid missed splits, namely incorrectly connecting curves that are not visible in the image. This is of high importance in our two use-cases, namely ultrasound image quality assessment, and road network segmentation. The first of these datasets provides a particularly challenging segmentation task, due to the low signal-to-noise ratio typical of ultrasound.

Our method is built around a dual-decoder network, which first makes a rough segmentation based on image texture, and next refines this optimizing for predicting correct topological structures. Here "correct" also emphasises the structure being visible in the image. As the second network takes the predicted foreground probabilities as input, it learns to enhance those responses that form curvilinear structures. This is obtained using self-supervised contrastive learning, to teach the network the difference between a weak curvilinear response, and no response. On the highly challenging ULTRASOUND dataset, we see that our method outperforms all other methods. In particular, we see that our method is particularly good at balancing false and missed splits. This is natural as most methods are developed using easier segmentation tasks such as e.g. blood vessel segmentation, and they are not optimized to handle the challenging nature of ultrasound data. On the ROAD dataset, our method is competitive with the other methods.

The validation is challenging on the ROAD dataset, where we are really looking at an instance segmentation task. Distances designed to detect the geometric similarity of curves, such as the Frechet distance, break down as they are forced to compare road segments that most certainly do not describe the same road. We do, however, see that our method outperforms the rest on pixel-based measures of overlap, and is competitive on the purely topological metrics.

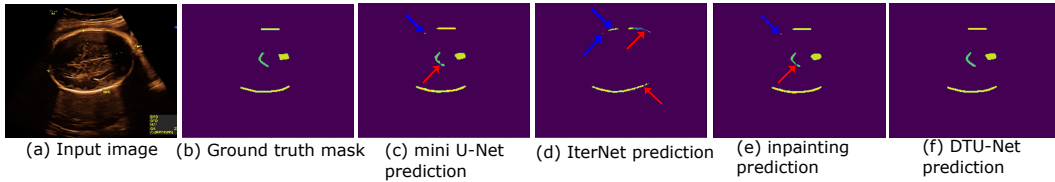


Figure 4: Segmentation results of different models on an example from the ULTRASOUND dataset. Disparate anatomies are colored differently. The blue arrows point at missed splits while the red arrows point at false splits in the image. Please zoom in for details.

One important difference between methods is the number of parameters used. We have designed most methods around the fixed size mini U-net. Since our own method has the additional topology network, it de facto has more parameters than the mini U-net trained with cIDice. To assess whether this difference in parameters was unfair, we also compared our method to a deeper U-net (with more parameters than our full architecture), trained with cIDice. However, the results (see Table 6) show that we still outperform cIDice on the ULTRASOUND dataset even when it is given the advantage of more parameters. The IterNet architecture also has more parameters than ours, but is not competitive on the ULTRASOUND dataset.

In summary, we have proposed a framework for segmenting curvilinear structures that are supported by the image content, and shown that it performs on par with the baselines on a common road network detection dataset, and that it outperforms the baselines by far on the very challenging ULTRASOUND dataset. We find it interesting that all baseline models struggle on the ultrasound data, and see this as a cue for the community to include more challenging segmentation tasks when developing methods for curvilinear structure segmentation.

References

- Alt, H. and Godau, M. (1995). Computing the fréchet distance between two polygonal curves. *International Journal of Computational Geometry & Applications*, 5(01n02):75–91.
- Bibiloni, P., González-Hidalgo, M., and Massanet, S. (2016). A survey on curvilinear object segmentation in multiple applications. *Pattern Recognition*, 60:949–970.
- Chen, L.-C., Papandreou, G., Kokkinos, I., Murphy, K., and Yuille, A. L. (2017). Deeplab: Semantic image segmentation with deep convolutional nets, atrous convolution, and fully connected crfs. *IEEE transactions on pattern analysis and machine intelligence*, 40(4):834–848.
- Chen, W., Yu, S., Wu, J., Ma, K., Bian, C., Chu, C., Shen, L., and Zheng, Y. (2020). Tr-gan: topology ranking gan with triplet loss for retinal artery/vein classification. In *International Conference on Medical Image Computing and Computer-Assisted Intervention*, pages 616–625. Springer.
- Clough, J. R., Byrne, N., Oksuz, I., Zimmer, V. A., Schnabel, J. A., and King, A. P. (2019). A topological loss function for deep-learning based image segmentation using persistent homology. *arXiv preprint arXiv:1910.01877*.
- Cubero-Fernandez, A., Rodriguez-Lozano, F., Villatoro, R., Olivares, J., Palomares, J. M., et al. (2017). Efficient pavement crack detection and classification. *EURASIP Journal on Image and Video Processing*, 2017(1):1–11.
- Deng, J., Dong, W., Socher, R., Li, L.-J., Li, K., and Fei-Fei, L. (2009). Imagenet: A large-scale hierarchical image database. In *2009 IEEE conference on computer vision and pattern recognition*, pages 248–255. Ieee.
- Dong, X. and Shen, J. (2018). Triplet loss in siamese network for object tracking. In *Proceedings of the European conference on computer vision (ECCV)*, pages 459–474.
- Frangi, A. F., Niessen, W. J., Vincken, K. L., and Viergever, M. A. (1998). Multiscale vessel enhancement filtering. In *International conference on medical image computing and computer-assisted intervention*, pages 130–137. Springer.
- Hermans, A., Beyer, L., and Leibe, B. (2017). In defense of the triplet loss for person re-identification. *arXiv preprint arXiv:1703.07737*.
- Hu, J., Shen, L., and Sun, G. (2018). Squeeze-and-excitation networks. In *Proceedings of the IEEE conference on computer vision and pattern recognition*, pages 7132–7141.
- Hu, X., Li, F., Samaras, D., and Chen, C. (2019). Topology-preserving deep image segmentation. *Advances in Neural Information Processing Systems*, 32.
- Jha, D., Riegler, M. A., Johansen, D., Halvorsen, P., and Johansen, H. D. (2020). Doubleu-net: A deep convolutional neural network for medical image segmentation. In *2020 IEEE 33rd International symposium on computer-based medical systems (CBMS)*, pages 558–564. IEEE.

- L. Srinidhi, C., Aparna, P., and Rajan, J. (2017). Recent advancements in retinal vessel segmentation. *Journal of medical systems*, 41(4):1–22.
- Li, L., Verma, M., Nakashima, Y., Nagahara, H., and Kawasaki, R. (2020). Internet: Retinal image segmentation utilizing structural redundancy in vessel networks. In *Proceedings of the IEEE/CVF Winter Conference on Applications of Computer Vision*, pages 3656–3665.
- Li, X., Wang, L., and Sung, E. (2008). Adaboost with svm-based component classifiers. *Engineering Applications of Artificial Intelligence*, 21(5):785–795.
- Lin, T.-Y., Goyal, P., Girshick, R., He, K., and Dollár, P. (2017). Focal loss for dense object detection. In *Proceedings of the IEEE international conference on computer vision*, pages 2980–2988.
- Long, J., Shelhamer, E., and Darrell, T. (2015). Fully convolutional networks for semantic segmentation. In *Proceedings of the IEEE conference on computer vision and pattern recognition*, pages 3431–3440.
- Mnih, V. (2013). *Machine Learning for Aerial Image Labeling*. PhD thesis, University of Toronto.
- Mosinska, A., Marquez-Neila, P., Koziński, M., and Fua, P. (2018). Beyond the pixel-wise loss for topology-aware delineation. In *Proceedings of the IEEE conference on computer vision and pattern recognition*, pages 3136–3145.
- Mou, L., Zhao, Y., Fu, H., Liu, Y., Cheng, J., Zheng, Y., Su, P., Yang, J., Chen, L., Frangi, A. F., et al. (2021). Cs2-net: Deep learning segmentation of curvilinear structures in medical imaging. *Medical image analysis*, 67:101874.
- Ronneberger, O., Fischer, P., and Brox, T. (2015). U-net: Convolutional networks for biomedical image segmentation. In *International Conference on Medical image computing and computer-assisted intervention*, pages 234–241. Springer.
- Safaei, N., Smadi, O., Masoud, A., and Safaei, B. (2022). An automatic image processing algorithm based on crack pixel density for pavement crack detection and classification. *International Journal of Pavement Research and Technology*, 15(1):159–172.
- Sasaki, K., Iizuka, S., Simo-Serra, E., and Ishikawa, H. (2017). Joint gap detection and inpainting of line drawings. In *Proceedings of the IEEE conference on computer vision and pattern recognition*, pages 5725–5733.
- Sato, Y., Nakajima, S., Shiraga, N., Atsumi, H., Yoshida, S., Koller, T., Gerig, G., and Kikinis, R. (1998). Three-dimensional multi-scale line filter for segmentation and visualization of curvilinear structures in medical images. *Medical image analysis*, 2(2):143–168.
- Schapire, R. E. (1999). A brief introduction to boosting. In *Ijcai*, volume 99, pages 1401–1406. Citeseer.
- Schroff, F., Kalenichenko, D., and Philbin, J. (2015). Facenet: A unified embedding for face recognition and clustering. In *Proceedings of the IEEE conference on computer vision and pattern recognition*, pages 815–823.
- Shit, S., Paetzold, J. C., Sekuboyina, A., Ezhov, I., Unger, A., Zhylka, A., Pluim, J. P., Bauer, U., and Menze, B. H. (2021). cldice-a novel topology-preserving loss function for tubular structure segmentation. In *Proceedings of the IEEE/CVF Conference on Computer Vision and Pattern Recognition*, pages 16560–16569.
- Simonyan, K. and Zisserman, A. (2014). Very deep convolutional networks for large-scale image recognition. *arXiv preprint arXiv:1409.1556*.
- Vega, R., Sanchez-Ante, G., Falcon-Morales, L. E., Sossa, H., and Guevara, E. (2015). Retinal vessel extraction using lattice neural networks with dendritic processing. *Computers in biology and medicine*, 58:20–30.
- Wang, X. and Jiang, X. (2018). Post-processing for retinal vessel detection. In *Tenth International Conference on Digital Image Processing (ICDIP 2018)*, volume 10806, page 1080656. International Society for Optics and Photonics.

- Wang, Y., Peng, Y., Liu, X., Li, W., Alexandropoulos, G. C., Yu, J., Ge, D., and Xiang, W. (2022). Ddu-net: Dual-decoder-u-net for road extraction using high-resolution remote sensing images. *arXiv preprint arXiv:2201.06750*.
- Wu, L., Cheng, J.-Z., Li, S., Lei, B., Wang, T., and Ni, D. (2017). Fuiqa: fetal ultrasound image quality assessment with deep convolutional networks. *IEEE transactions on cybernetics*, 47(5):1336–1349.
- Xu, Z., Sun, Y., Wang, L., and Liu, M. (2021). Cp-loss: Connectivity-preserving loss for road curb detection in autonomous driving with aerial images. In *2021 IEEE/RSJ International Conference on Intelligent Robots and Systems (IROS)*, pages 1117–1123. IEEE.
- Yusof, N., Osman, M., Noor, M., Ibrahim, A., Tahir, N., and Yusof, N. (2018). Crack detection and classification in asphalt pavement images using deep convolution neural network. In *2018 8th IEEE International Conference on Control System, Computing and Engineering (ICCSCE)*, pages 227–232. IEEE.
- Zhang, H. and Lui, L. M. (2022). Topology-preserving segmentation network: A deep learning segmentation framework for connected component. *arXiv preprint arXiv:2202.13331*.
- Zhang, Z., Liu, Q., and Wang, Y. (2018). Road extraction by deep residual u-net. *IEEE Geoscience and Remote Sensing Letters*, 15(5):749–753.